Effects of Track-Seeking Motion on the Flying Attitudes of Ultralow Flying Sliders

Jia-Yang Juang [1], Hiroyuki Kubotera [2] and David B. Bogy [1]

(1) Computer Mechanics Laboratory
Department of Mechanical Engineering
University of California at Berkeley
Berkeley, CA 94720

(2) Magnetic Disk Drive Laboratory
Storage Intelligent System Laboratory
Fujitsu Laboratories Ltd.
Japan

ABSTRACT

The flying height (FH) change during a track-seeking motion becomes of significant concern for ultralow flying sliders. The presence of nanoscale adhesion forces, such as intermolecular and electrostatic forces, can adversely decrease the FH and even cause head-disk impact. A quasi-static approximation of track-seeking motion is proposed here, which if sufficiently accurate can substantially decrease the computation time over that required for a dynamic analysis. The track-seeking performances of four different air bearing surface (ABS) designs are numerically investigated by the quasi-static approximation, and the results are compared with those computed by the CML Dynamic Simulator. The former gives good agreements with the latter but with much less computation effort. The effects of various factors causing FH changes are presented and compared quantitatively. The effective skew angle is found to be the dominant factor, but the inertia effect is also not negligible. Two designs, called Scorpion III and IV, designed previously as active FH control sliders, are

found to exhibit an enhancement in track-seeking performance, compared with two other conventional ABS designs.

1. INTRODUCTION

As the spacing between the slider and the disk decreases in hard disk drives, the linear bit spacing of magnetic recording can decrease, resulting in a higher areal density. A physical spacing (or gap flying height, gap FH) of less than 5 nm between the read/write element and the surface of the disk is required for ultrahigh density recording. For such ultralow flying sliders the changes in FH during track-seeking motions not only cause signal loss, but also significantly increase the risk of head-disk contact. Moreover, the presence of nanoscale adhesion forces, such as intermolecular and electrostatic forces, can cause dynamical instability. In order for a reliable head-disk interface to be maintained the FH change and contact between the slider and disk have to be avoided. Different ABS designs can perform quite differently during the track-seeking process. Therefore, the dynamic track-seeking performance of air bearing sliders is becoming of increasing importance. A better understanding of the factors that cause FH change should help improve the ABS design to achieve better track-seeking performance.

Cha *et al.* [1] studied the FH change during seek operation for TPC (transverse pressure contour) sliders. They suggested that at high seek velocities the skew angle effect dominates over the inertia effect but there was no quantitative comparison between the cases with and without inertia effects due to the difficulty of measuring FH during track-seeking and the absence of proper dynamic simulators. Liu and Soh [2] experimentally investigated the effects of track-seeking velocity on air bearing skew angle, air flow speed and flying performance of TPC and Tri-pad sliders. The effects of the slider's inertia and acceleration

were not considered. Chen and Bogy [3] carried out a numerical study of the track-seeking dynamics of the picosized TNPS and U sliders using the CML Dynamic Simulator. They found that the two sliders had distinct dynamic characteristics. The Dynamic Simulator included the inertia effect and provided more comprehensive simulations of track-seeking dynamics but it required much more computation time. In a recent paper by Dorius *et al.* [4], the gap FHs of a pico and femto slider were forced to drop about 20 and 10 %, respectively, during track seeking.

In this report we propose a quasi-static approximation of the track-seeking motion, which includes the effects of HGA inertia, effective skew angles and nanoscale adhesion forces in the HDI. We first compare the track-seeking simulations of four ABS designs by quasi-static approximation with those obtained using the CML Dynamic Simulator on a smooth disk surface. Then we quantitatively study the effects of various factors on the FH change.

2. THEORETICAL BACKGROUND AND NUMERICAL METHODS

2.1 Air Bearing Slider and Suspension Dynamics

The pressure distribution between the slider and the rotating disk can be described by the compressible Reynolds equation. The non-dimensionalized generalized Reynolds equation can be written as follows:

$$\frac{\partial}{\partial X}\left[\hat{Q}PH^3\frac{\partial P}{\partial X}-\Lambda_X PH\right]+\frac{\partial}{\partial Y}\left[\hat{Q}PH^3\frac{\partial P}{\partial Y}-\Lambda_Y PH\right]=\sigma\frac{\partial}{\partial T}[PH] \qquad (1)$$

where $\Lambda_X = 6\mu UL / p_a h_m^2$ and $\Lambda_Y = 6\mu VL / p_a h_m^2$ are the bearing numbers in the x and y directions, $\sigma = 12\mu\omega L^2 / p_a h_m^2$ is the squeeze number, μ is the viscosity, p_a is the ambient pressure, and $\hat{Q}$ is the Poiseuille flow factor.

The equations of motion of an air bearing slider flying over a rotating disk are:

$$\begin{aligned} m\ddot{z} &= F + \int_A (p - p_a) dA \\ I_\theta \ddot{\theta} &= M_\theta + \int_A (p - p_a)(x_g - x) dA \\ I_\phi \ddot{\phi} &= M_\phi + \int_A (p - p_a)(y_g - y) dA \end{aligned} \tag{2}$$

where z, θ, and ϕ are the vertical displacement, pitch, and roll, respectively. I_θ and I_ϕ are the moments of inertia, x_g and y_g are the positions of the slider's center of gravity, and F, M_θ and M_ϕ are the force and moments exerted on the slider by the suspension. For track-seeking motions, M_θ and M_ϕ include the contribution of the inertia forces.

The CML Dynamic Air Bearing Simulator was developed to solve the generalized Reynolds equations (1) coupled with the dynamics of the slider body (2) and a lumped parameter suspension, where the suspension is represented by flexure stiffness and damping coefficients. By using the simulator, we can obtain the dynamic flying attitude of a slider during track-seeking motions. However, since the time step used in the dynamic simulation is usually on the order of 1×10^{-7} s, it requires considerable computation effort to conduct one track-seeking simulation with an average seeking time of 11 ms.

2.2 Quasi-Static Approximation of Track-Seeking Motion

In order to reduce the computation effort of track-seeking simulations and quantitatively study the contribution of various factors on the FH change during track-seeking, we carried out a quasi-static approximation of the track-seeking motion. Instead of

simultaneously solving Eq. (1) and (2) at each time step, we solve Eq. (1) under static suspension loading with consideration of the seeking velocity and HGA inertia at different radial positions during track-seeking. The change of seeking velocity causes changes of skew angle and air flow speed and direction. The geometrical skew angle refers to the angle between the slider's longitudinal axis and the track direction. The effective skew angle is the angle between the slider's longitudinal direction and the relative disk velocity (or air flow velocity) which is the resultant vector of the disk track linear velocity and the slider's seeking velocity. As the seeking velocity increases, the difference between the geometrical and effective skew angles increases.

The acceleration of the center of gravity of a slider during track-seeking can be expressed as

$$a = a_t e_t + a_n e_n = a_t e_t + \left(\omega^2 r\right) e_n \tag{3}$$

where a_t and a_n are the tangential and normal components, respectively. ω and r are the angular velocity of the arm and the arm length of the VCM actuator, respectively. The tangential component is also referred to as the seeking acceleration. Since the inertia effect of the suspension has minimal effect on the roll angle and FH, only the inertia of the slider is considered in this study. The additional torques exerted on the slider body due to these inertia forces can be written as

$$\Delta M_\theta = -m \cdot a_n \cdot \frac{h}{2}; \quad \Delta M_\phi = -m \cdot a_t \cdot \frac{h}{2} \tag{4}$$

where m and h are the mass and thickness of the slider.

3. RESULTS AND DISCUSSIONS

3.1 Air Bearing Designs and Track-Seeking Performances

In this report, we study the track-seeking performances of four ABS designs that incorporate subambient pressure regions. Their drive and air bearing specifications are summarized in Table I. The first design, depicted in Fig. 1(a), is a five-pad design labeled ABS I. It was designed using an optimization algorithm [5] for a nearly uniform 5-nm FH across the disk. The region of pole-tip recession in the original design was removed for a more realistic calculation of the nanoscale adhesion forces in the HDI. The second and more complicated design is shown in Fig. 2(a) and labeled ABS II. Figures 1(b) and 2(b) show the pressure profiles normalized by the ambient pressure generated under the ABS I and ABS II sliders, respectively. The sliders are mainly supported by the high pressure peaks generated by the central trailing pads, which are typically used in commercial products. The third and fourth designs, named Scorpion III and Scorpion IV, were designed as actively controlled-FH sliders with thermal and piezoelectric nanoactuators [6], [7], respectively. For a controlled-FH slider, the FH is about 10 nm in the off duty cycle (passive mode) and is reduced to ~2 nm during reading and writing (active mode) by applying either a current or a voltage to an active element, such as a resistive heating element or piezoelectric material. As shown in Figs. 3(a) and 4(a), the areas of their central trailing pads have been significantly reduced to increase the actuation efficiency. The pressure distributions exhibit distinct features compared to conventional designs as shown in Figs. 3(b) and 4(b). The high pressures generated at the side rails of Scorpion III and IV support the sliders and help achieve high stiffness, especially in the roll direction, and constant roll angles over the disk. The increase of roll stiffness can effectively reduce variations of roll angle due to inertia forces during

track-seeking motions. Therefore decrease in the minimum FH are held to a minimum. The features of the two ABS pads near the trailing edge of Scorpion III or IV help generate high pressure and large negative force, which are expected to reduce the sensitivity of the FH to the change of skew angle. A summary of the flying attitudes, air bearing stiffness and negative forces at the MD is given in Table II.

Figures 5, 6 and 7 illustrate the track-seeking profiles used in this study. The maximum seeking acceleration is 637 m/s^2 (or 65 G) for all of the four ABS designs and the other parameters, such as velocity, radial position, geometrical and effective skews are determined by the length of the VCM actuator and the distance between the pivot and the center of the disk according to specifications of each product. The simulation starts with an outward seek that is followed by an inward seek, thus completing a full-stroke seeking loop. For the outward seeking process of ABS I, the slider is first accelerated to -2.548 m/s in 4 ms (the minus sign indicates that the direction of seek motion is from ID to OD), followed by 1 ms of constant velocity, then it is decelerated to zero velocity in 4 ms. During the seek the geometrical skew angle changes from -1.211 to 13.999 degrees. For the inward seek, we simply reverse the outward seeking process. Although the actual seeking profile in disk drives may be different from that shown in Fig. 5, the major characteristics of track-seeking motion are contained in the profiles used in this study.

Figures 8, 9, 10 and 11 illustrate comparisons of gap FHs, pitch and roll angles during the corresponding full-stroke seeking loop between dynamic simulations and the quasi-static approximations introduced here for the ABS I, ABS II, Scorpion III, and Scorpion IV sliders, respectively. It is seen that for all the designs the quasi-static approximations demonstrate good agreements with the dynamic simulations. The inertia effect is clearly seen in the roll

and FH curves. It is noted that the Scorpion III and IV sliders exhibit extremely small FH, pitch and roll variations caused by the track-seeking motion, which can significantly reduce the risk of head-disk contact during track-seeking motion.

3.2 Factors Causing FH Change During Track-Seeking Motion

To investigate the contribution of effective skew, inertia and air flow speed to the FH change during a track-seeking motion, we performed both outward and inward quasi-static simulations of the ABS I slider with different combinations of the various factors. Fig. 12(a) shows the minimum FH change when the slider moves from ID to OD with the acceleration profile described in Fig. 5(a). The curve labeled “Track-following” shows the FH without seeking. The curve labeled “with roll and pitch torques” includes the effects of tangential (roll torque) and normal acceleration (pitch torque), effective skew and air flow speed. This is used as a baseline for comparing the contributions of the factors. It is observed that the FH drops about 1.5 nm near the MD. The effect of effective skew angle on the FH drop is the difference between the curve “Track-following” and the curve “w/o inertia”. It is clearly seen that the skew angle change is the dominant factor that causes the FH change during track-seeking. The contributions of the other factors are shown in Fig. 12(b). The error is defined as the ratio of the FH difference to the baseline value. The result without the inertia effect has an error of 12 % near the radial position of 19 mm, which is attributed to the roll angle change. The effect of centrifugal forces caused by normal acceleration has an error of less than 5 % and the effect of the change of the air flow speed has an error of less than 2 %. Similarly, Fig. 13 shows the minimum FH change when the slider moves from OD to ID. In this case, the inertia effect is found to be comparable to the effect of skew angle change.

The FH changes as a function of skew angle for the ABS I, ABS II, Scorpion III and Scorpion IV sliders are shown in Figs. 14 and 15. It is seen that the FHs of Scorpion III and IV are quite insensitive to skew angle as compared with ABS I and ABS II. In Fig. 15, the minimum FH of Scorpion IV is reduced to 5 nm with a 4-nm actuation stroke.

In order to study the effect of intermolecular and electrostatic forces on the minimum FH during track-seeking motion we performed quasi-static simulations for ABS I and Scorpion IV with a 4-nm actuation stroke in the presence of these forces. The effect of intermolecular forces was included with a nominal value of the Hamaker constant ($A = 8.9\times10^{-20}$ J) and the electrostatic forces were added with different electrical potentials (V = 0, 0.3 and 0.6 V) between the slider and the disk. The minimum FHs of ABS I and Scorpion IV are shown in Fig. 16(a) and (b), respectively. A comparison of the FH drops under the influence of intermolecular forces and an electrical potential of 0.6 V is also illustrated in Fig. 16 (c). It is seen that the FH of ABS I drops over 30 % near the radial position of 19 mm while Scorpion IV exhibits a much smaller and more uniform FH drop of less than 10 %.

4. CONCLUSION

This report proposes a quasi-static approximation of the track-seeking motion, which includes the effects of HGA inertia, effective skew angles and nanoscale adhesion forces in the HDI. The track-seeking simulations of four ABS designs by the quasi-static approximation give good agreements with those by the CML Dynamic Simulator but with much less computation effort. A quantitative study of the effects of various factors on the minimum FH change during track-seeking shows that the effective skew angle is dominant but the inertia effect is not negligible. Intermolecular and electrostatic forces were found to add to the FH drop of ABS I during the track-seeking. However, even with an electrical

potential of 0.6 V and intermolecular forces, the FH drop of Scorpion IV remains less than 10%. Even though the FH change and the adverse effect of these forces during track-seeking cannot be completely attenuated, a properly designed air bearing slider that decreases its sensitivity to skews, minimizes these forces and increases the roll stiffness can greatly enhance the track-seeking performance.

ACKNOWLEDGEMENT

This study is supported by the Computer Mechanics Laboratory (CML) at the University of California, Berkeley and Information Storage Industry Consortium (INSIC). J. Y. Juang has also been supported by The California State Nanotechnology Fellowship.

REFERENCES

1. E. Cha, C. Chiang and J. J. K. Lee, “Flying height change during seek operation for TPC sliders,” *IEEE Trans. Magn.*, vol. 31, pp. 2967-2969, 1995.
2. B. Liu and S. H. Soh, “Effects of seeking velocity on air bearing skew angle, air flow speed and flying performance of sliders with different ABS designs,” *IEEE Trans. Magn.*, vol. 32, pp. 3693-3695, 1996.
3. L. S. Chen and D. B. Bogy, “A numerical study of the track-seeking dynamics of the 30% TNPS and U sliders on smooth and laser-textured disks,” Technical Report No. 1998-007, Computer Mechanics Lab., Department of Mechanical Engineering, University of California, Berkeley.
4. L. Dorius, S. Bolasna, J. Kotla, R. Simmons, Y. Iihara, T. Matsumoto, A. Tobari, and H. Tsuchida, “Introduction of femto slider in mobile disk drives,” *IEEE Trans. Magn.*, vol. 40, pp. 349-352, 2004.
5. H. Zhu and D. B. Bogy, “Hard disc drive air bearing design: modified DIRECT algorithm and its application to slider air bearing surface optimization,” *Tribol. Intl.*, vol. 37, pp. 193-201, 2004.
6. J. Y. Juang and D. B. Bogy, “Air bearing surface design for flying control sliders with thermal actuation,” (in preparation).
7. J. Y. Juang, D. B. Bogy, and C. S. Bhatia, “Air bearing surface design for flying height control slider with piezoelectric nanoactuator,” Technical Report No. 2005-012, Computer Mechanics Lab., Department of Mechanical Engineering, University of California, Berkeley

TABLE I
AIR BEARING SPECIFICATIONS

	ABS I [a]	ABS II	Scorpion III [b]	Scorpion IV [c]
Form-Factor	Pico	Femco	Pico	Pico
Technology	N/A	Contact Start-Stop	Load/Unload	Load/Unload
Disk Speed (rpm)	7200	7200	15000	15000
Gram-Load (gf)	1.5	2.5	2.0	2.0
Crown (nm)	25.4	0	9.3	9.3
Camber (nm)	2.5	0	-2	-2
Etch Steps	2	4	2	3
Base Recess (μm)	2.5	4.75	1.7	1.7

TABLE II
COMPARISON OF FLYING ATTITUDES AND AIR BEARING STIFFNESS AT THE MD

	FH (nm)	Pitch (μrad)	Roll (μrad)	k_z (gf/nm)	k_p (μN.m/μrad)	k_r (μN.m/μrad)	Negative force (gf)
ABS I	6.3	202	-0.6	0.178	0.537	0.059	-3.1
ABS II	12.3	104	3.5	0.176	0.404	0.031	-3.5
Scorpion III	10.4	124	-0.3	0.328	1.036	0.403	-4.7
Scorpion IV	9.8	109	-0.4	0.182	0.517	0.246	-3.1

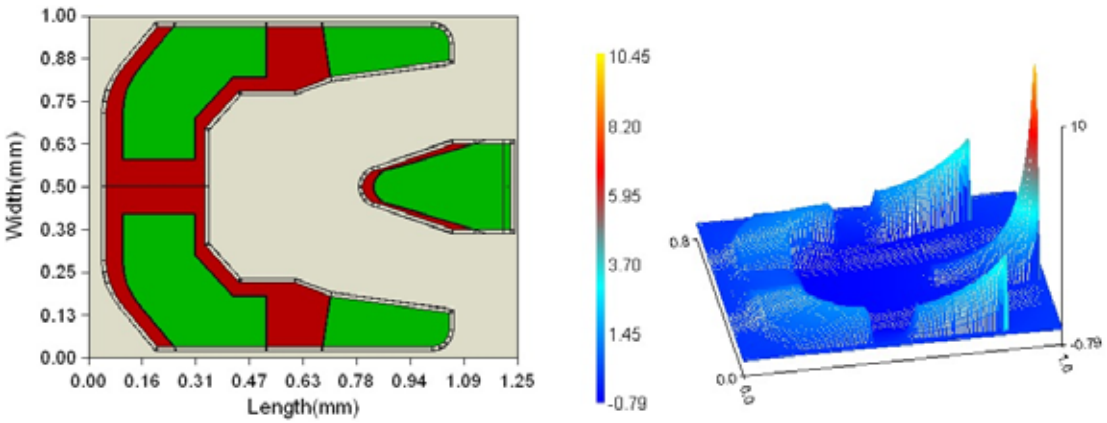

(a) (b)

Fig. 1. (a) Air bearing surface of a pico-slider, ABS I (1.25×1×0.3 mm); (b) Air bearing pressure profile at the MD (radial position: 21 mm, skew: 6.8248 ^{o}). The scale displayed is normalized to ambient pressure: $(p - p_a)/p_a$.

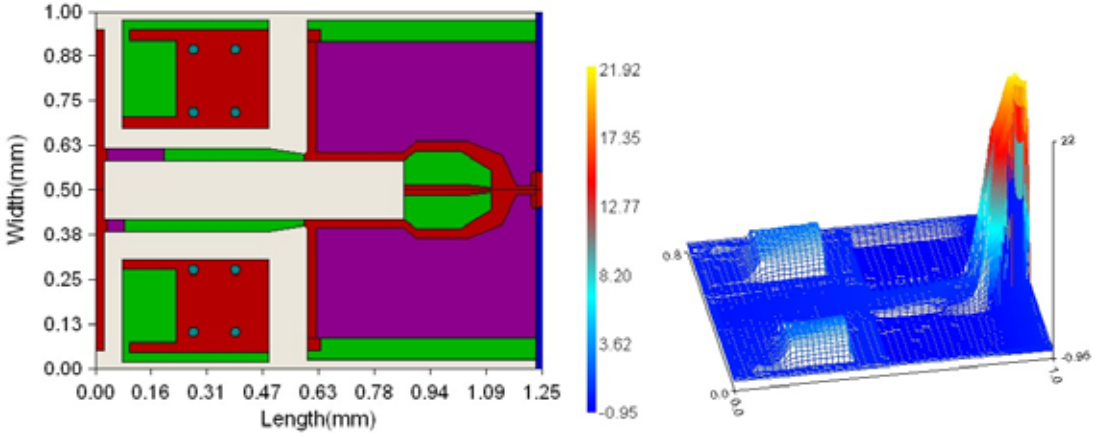

(a) (b)

Fig. 2. (a) Air bearing surface of a femco-slider (1.25×1×0.2 mm), ABS II; (b) Air bearing pressure profile at the MD (radial position: 31 mm, skew: 2.48 ^{o}).

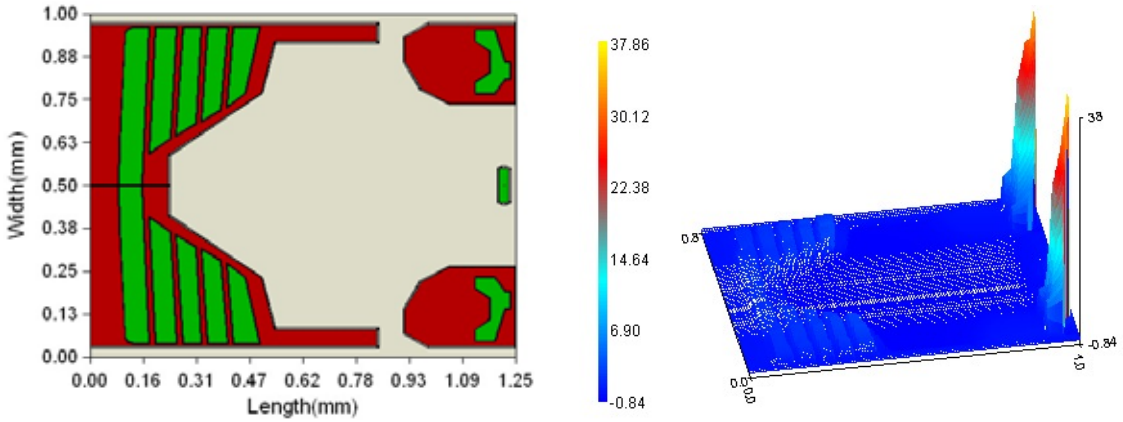

(a) (b)

Fig. 3. (a) Air bearing surface of a pico-slider, Scorpion III; (b) Air bearing pressure profile at the MD (radial position: 23.88 mm, skew: -2.56°).

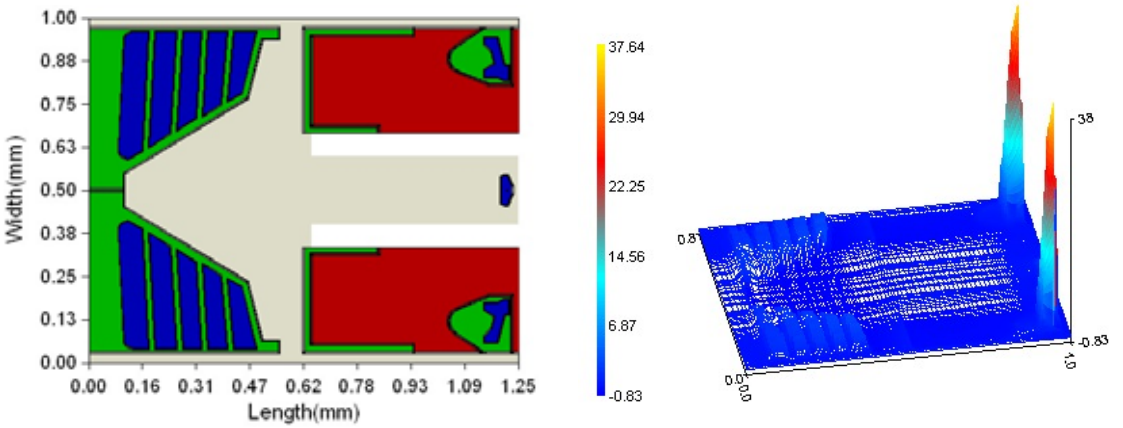

(a) (b)

Fig. 4. (a) Air bearing surface of a pico-slider, Scorpion IV; (b) Air bearing pressure profile at the MD (radial position: 23.88 mm, skew: -2.56°).

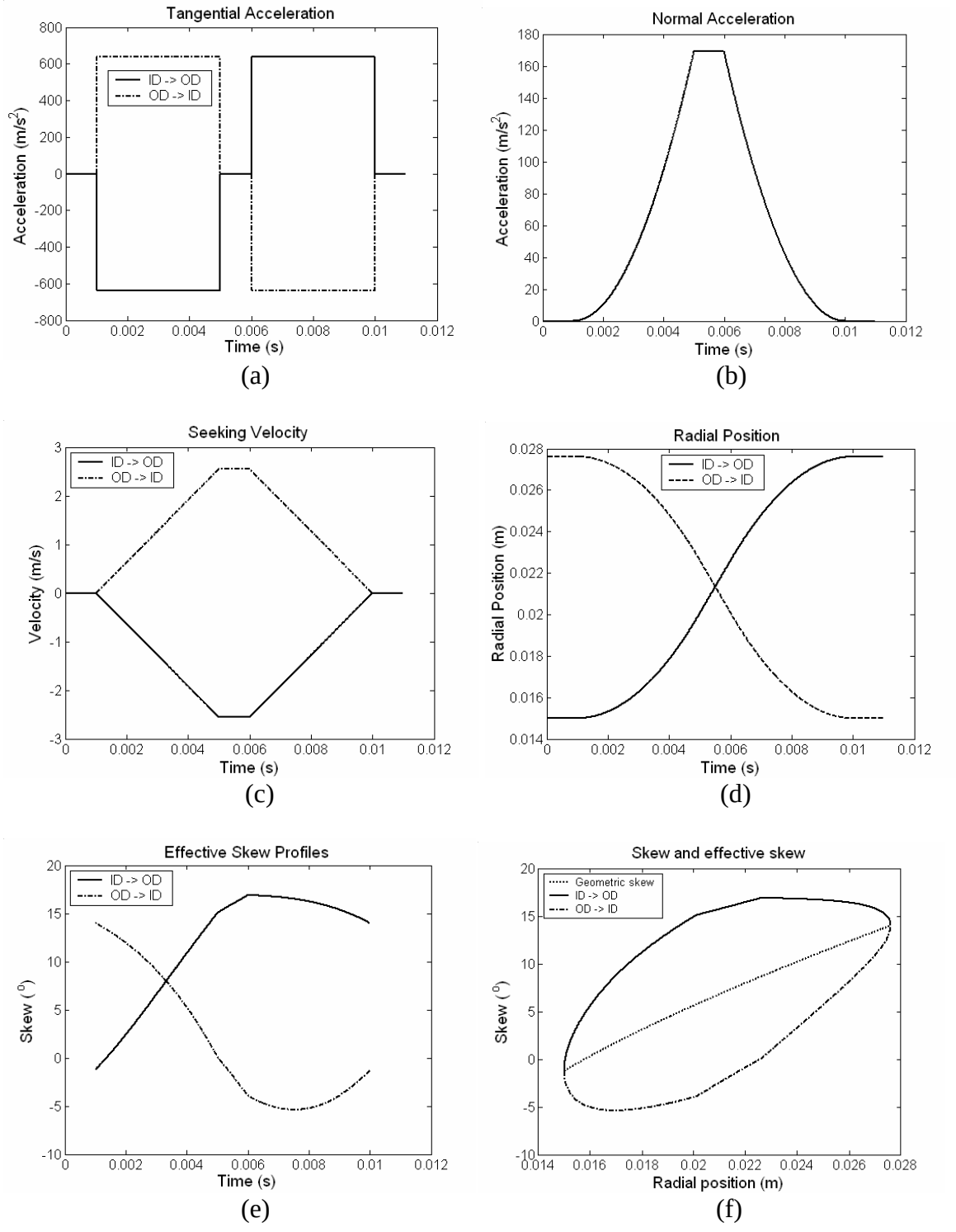

Fig. 5. Track-seeking profiles for ABS I. The maximum acceleration is 637 m/s^2 (or 65 G).

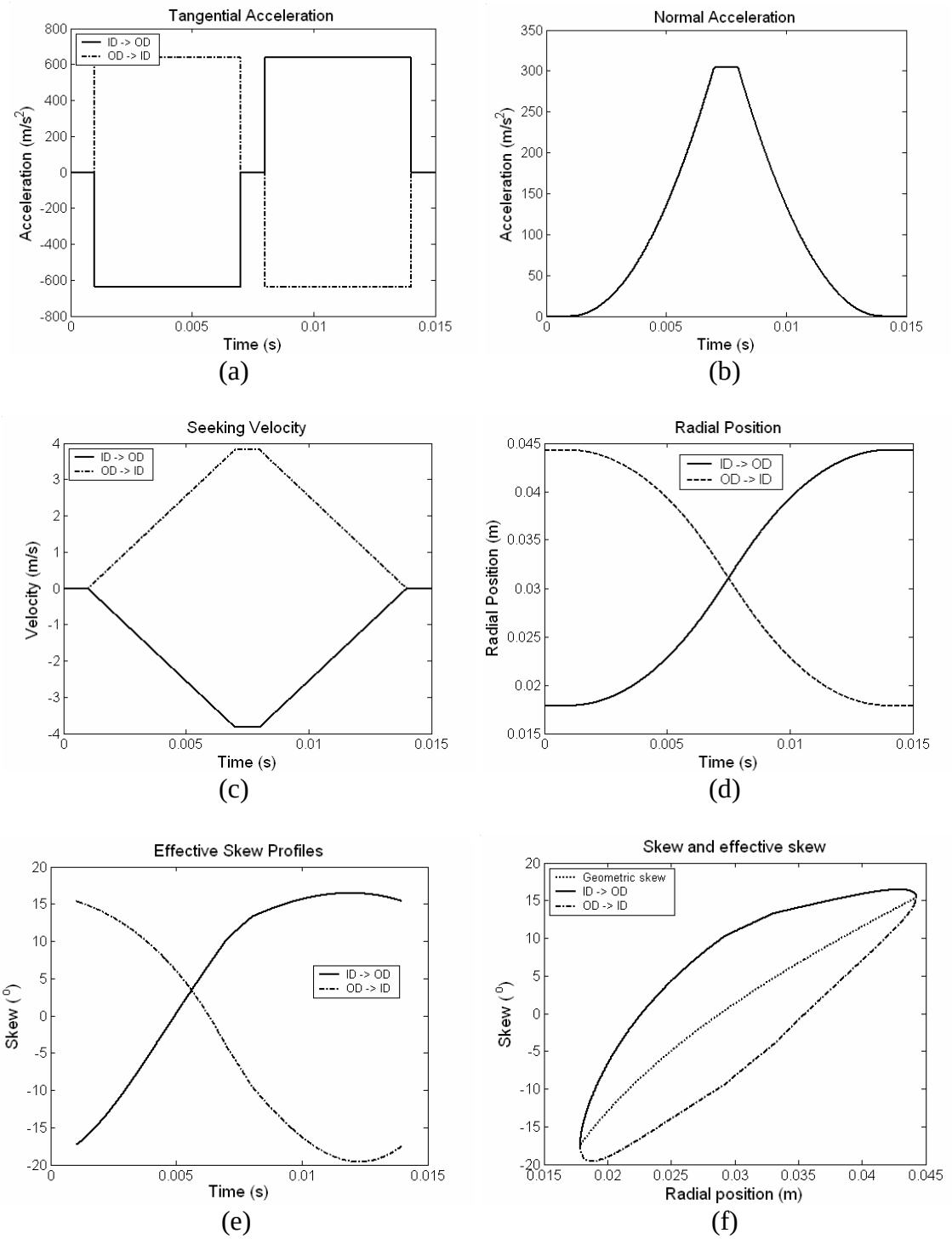

Fig. 6. Track-seeking profiles for ABS II. The maximum acceleration is 65 G.

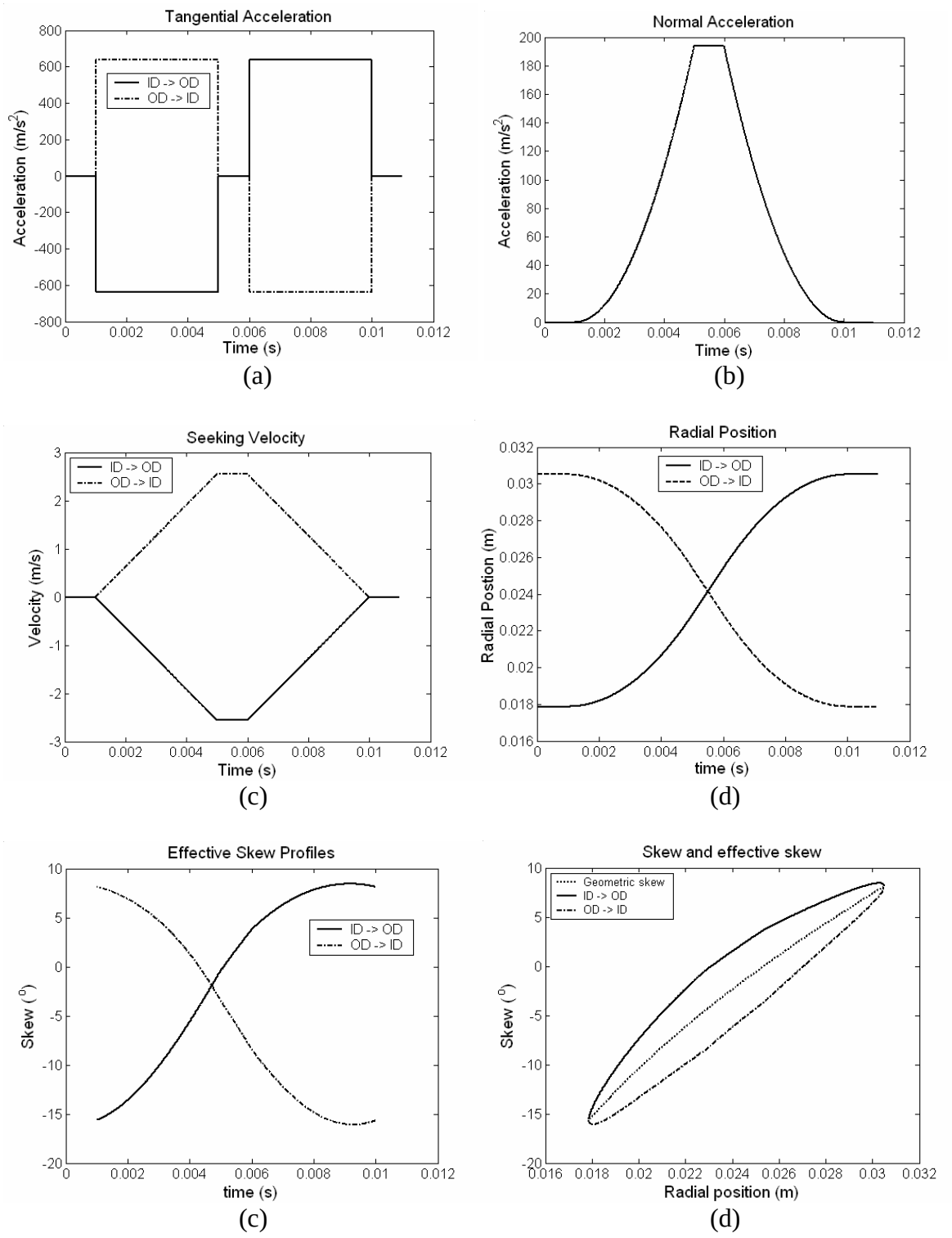

Fig. 7. Track-seeking profiles for Scorpion III and IV. The maximum acceleration is 65 G.

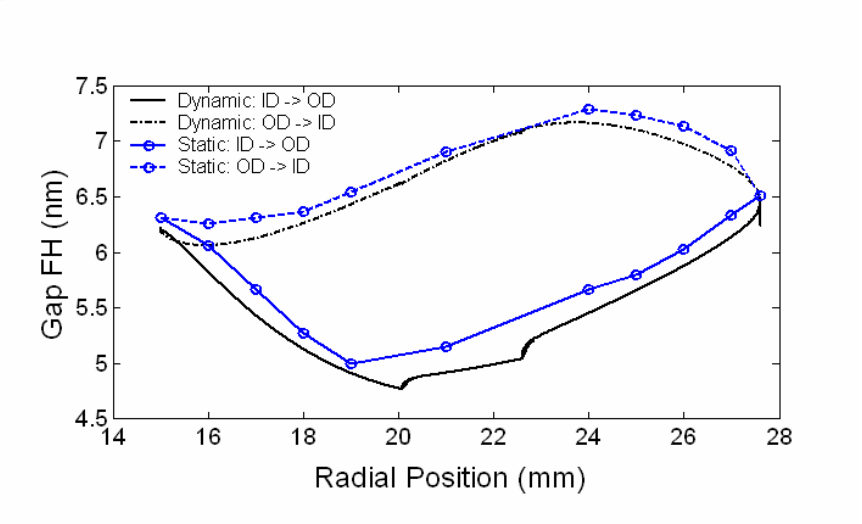

(a)

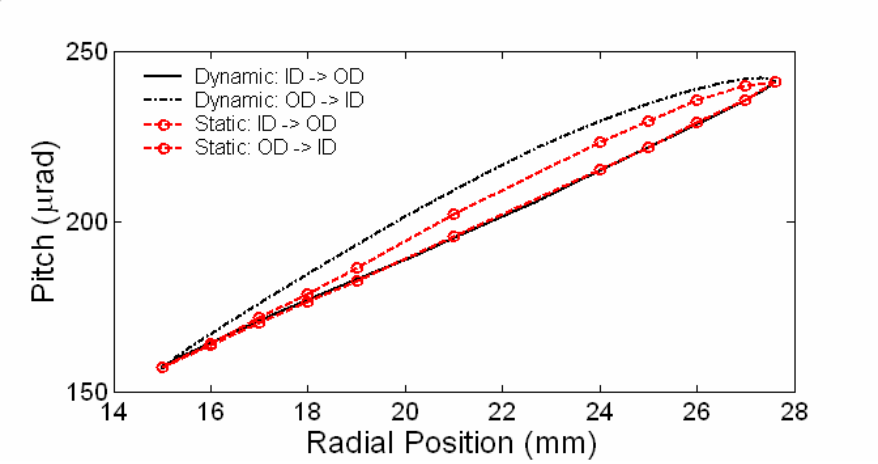

(b)

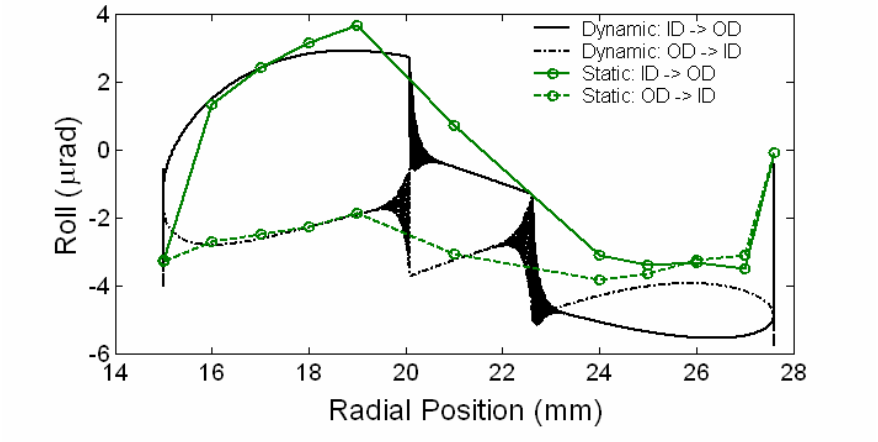

(c)

Fig. 8. Track-seeking performance of ABS I.

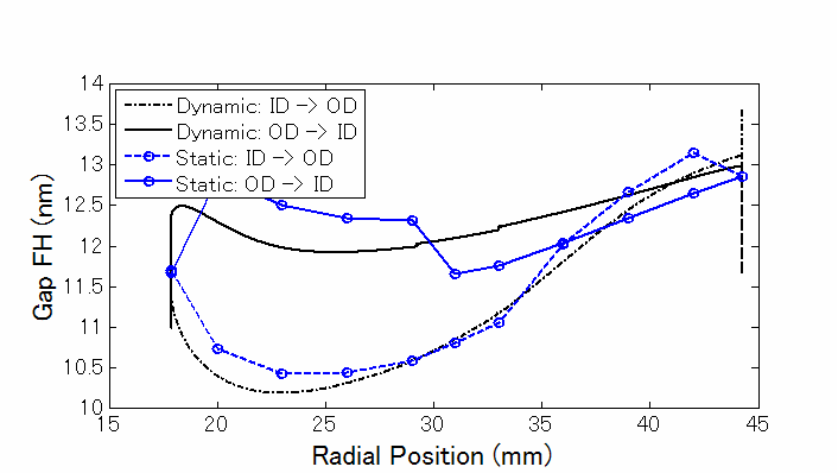

(a)

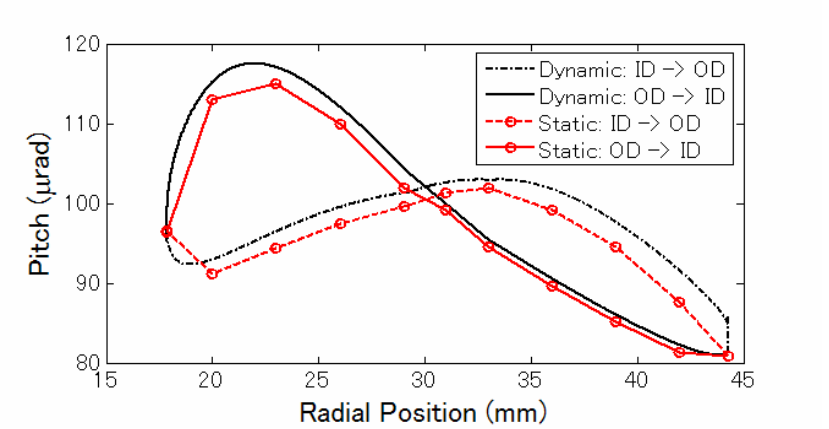

(b)

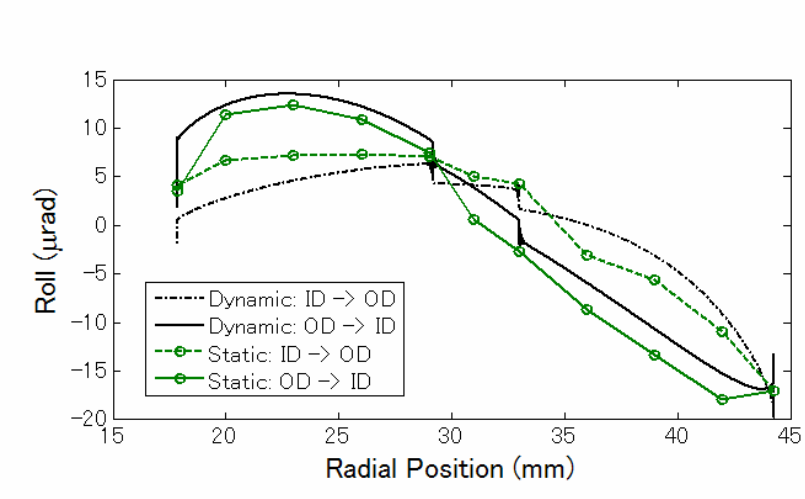

(c)

Fig. 9. Track-seeking performance of ABS II.

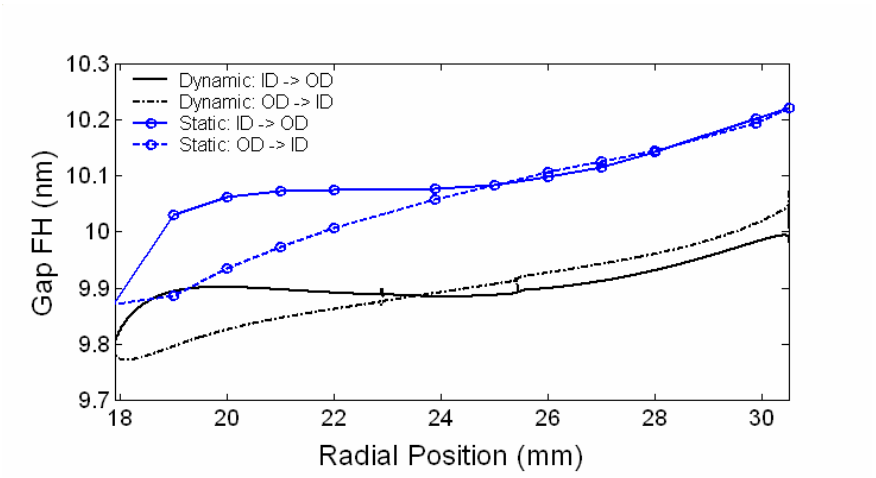

(a)

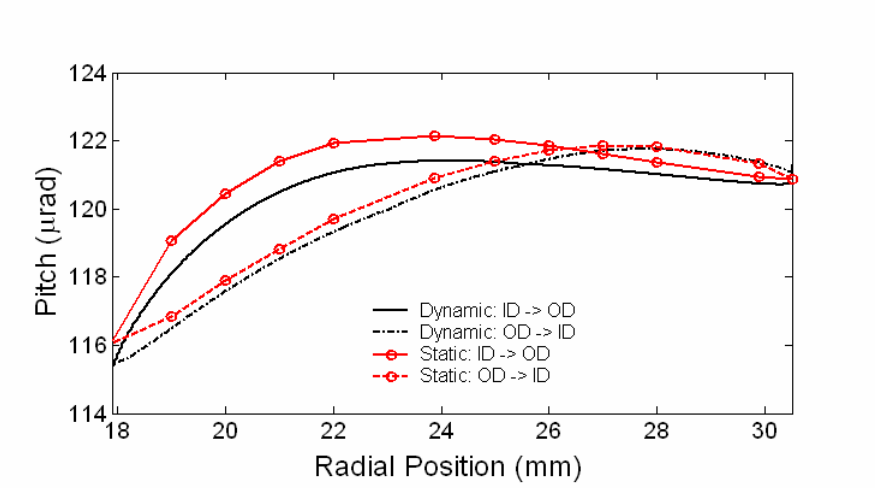

(b)

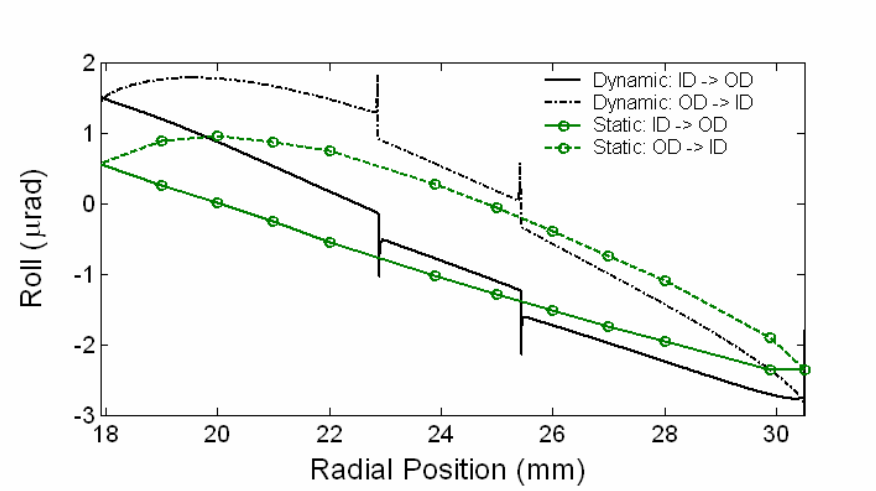

(c)

Fig. 10. Track-seeking performance of Scorpion III.

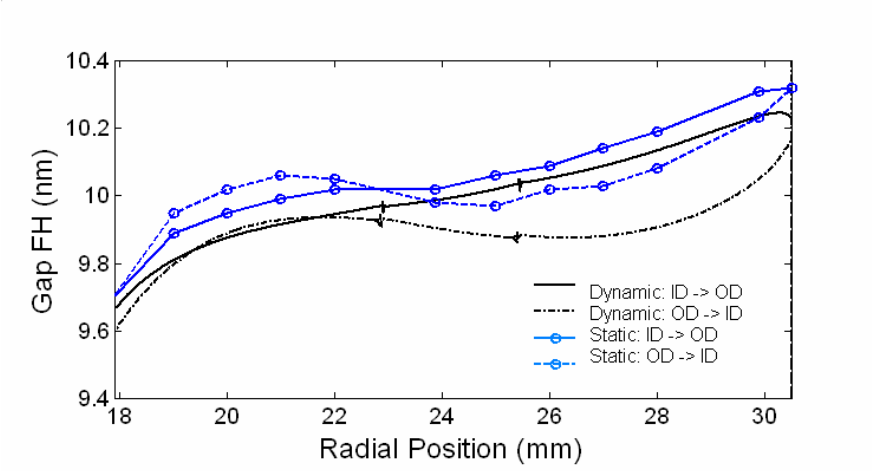

(a)

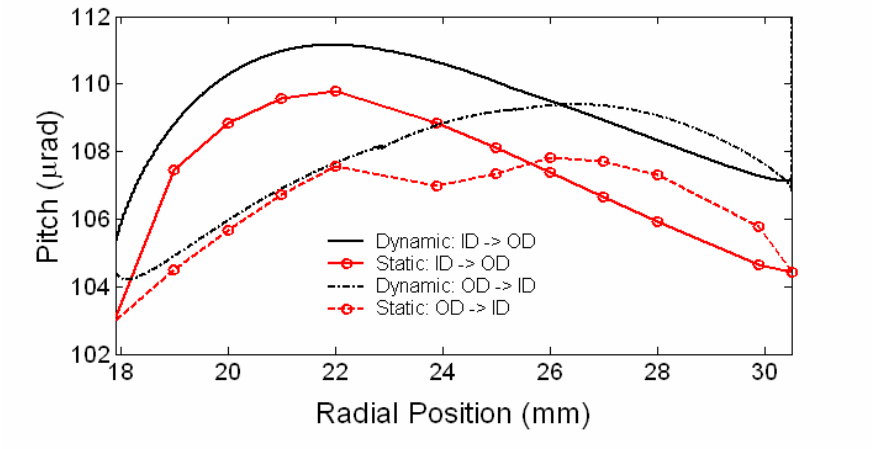

(b)

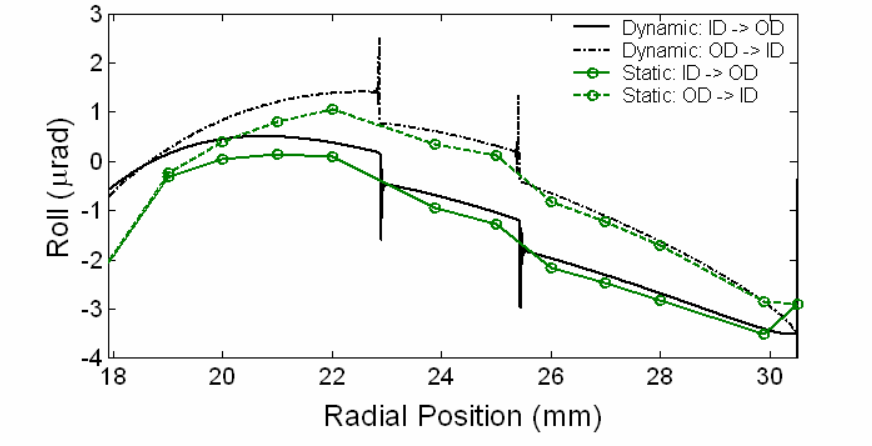

(c)

Fig. 11. Track-seeking performance of Scorpion IV.

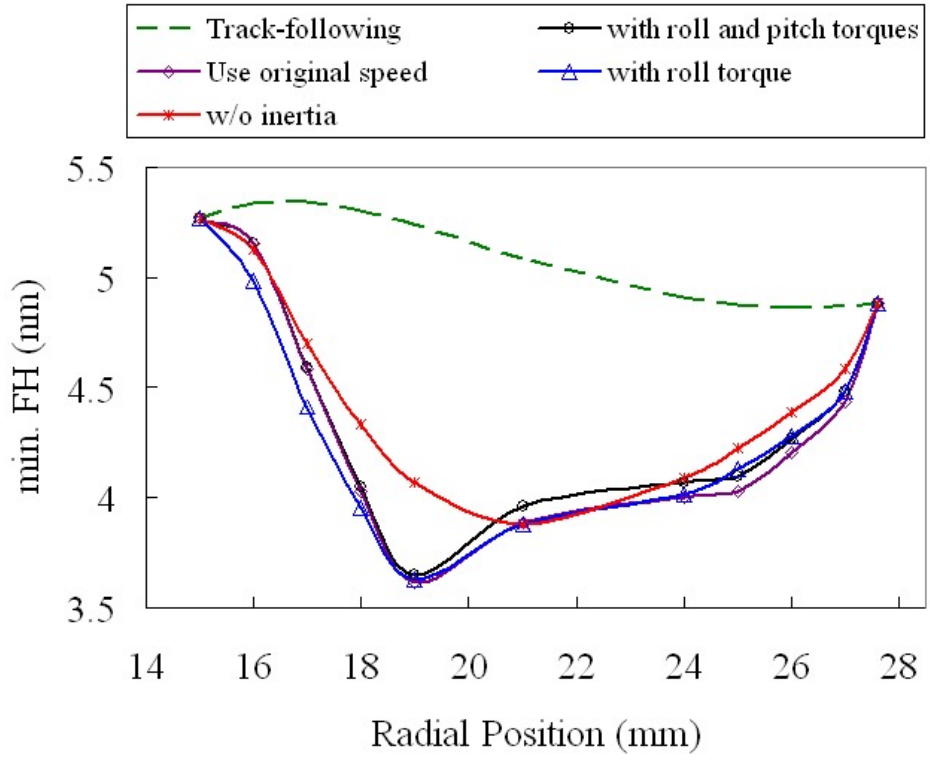

(a)

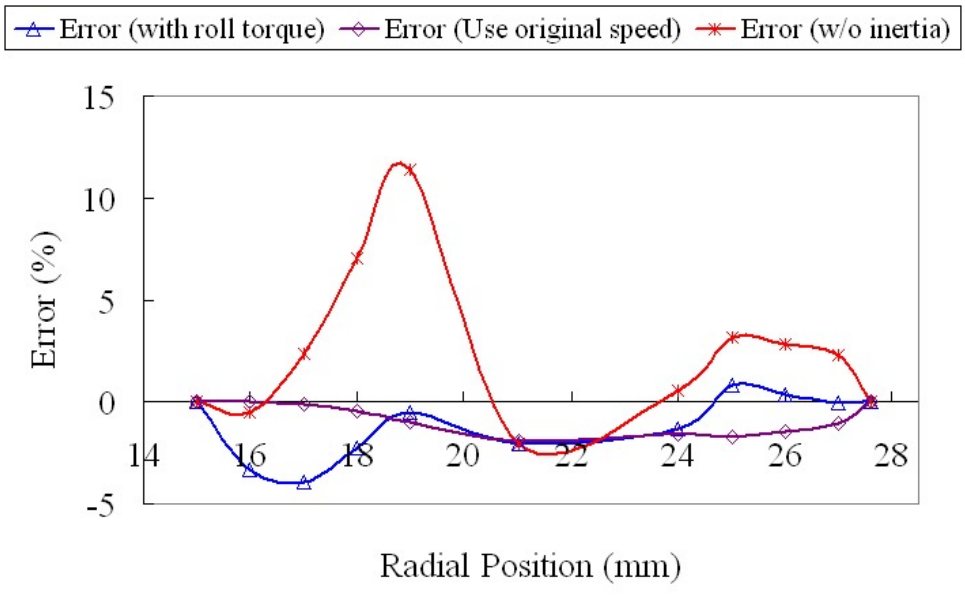

(b)

Fig. 12. Effects of the effective skew, inertia forces, and air flow speed on the FH changes of ABS I seeking from ID to OD. The error is calculated by subtracting the values of various curves from the baseline “with roll and pitch torques”.

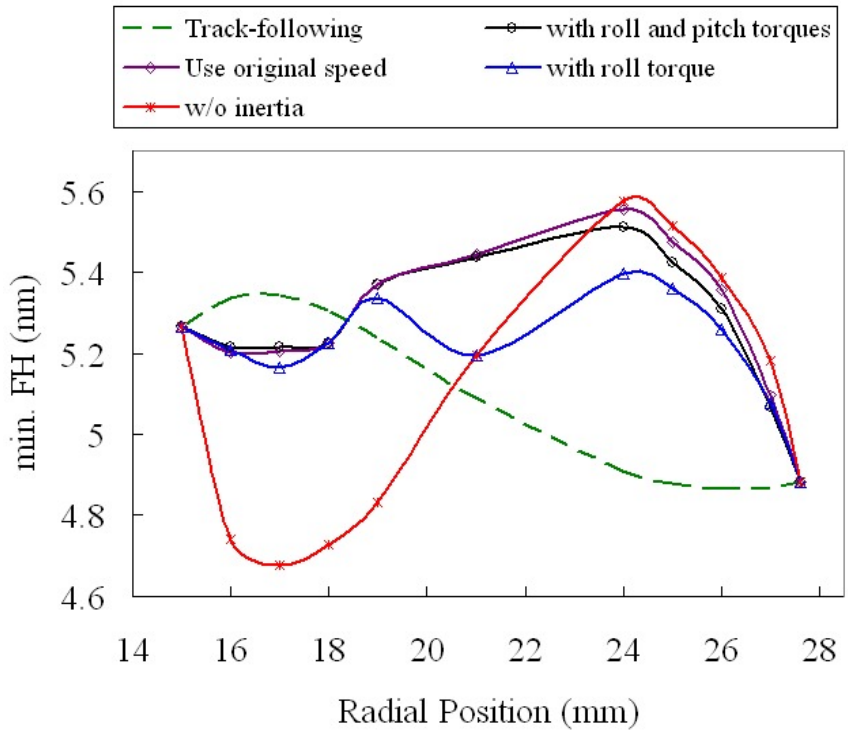

(a)

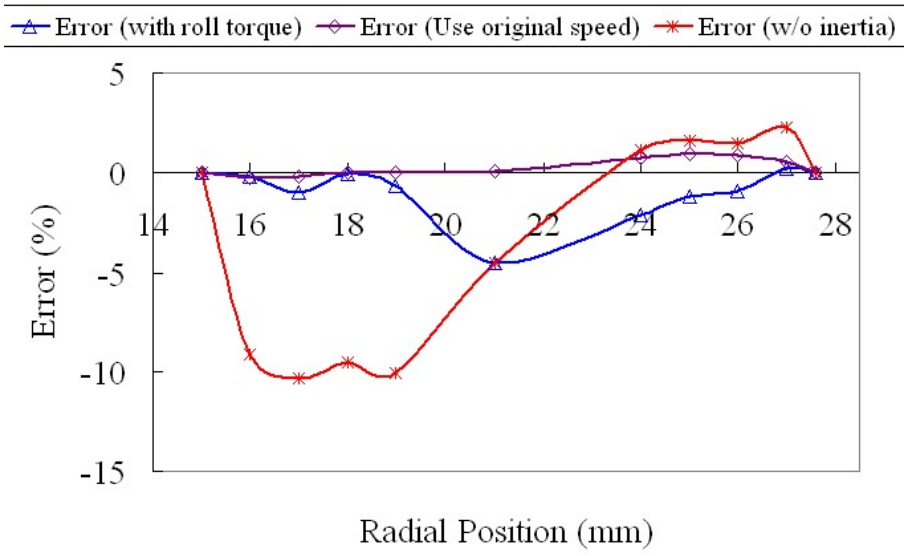

(b)

Fig. 13. Effects of the effective skew, inertia forces, and air flow speed on the FH changes of ABS I seeking from OD to ID.

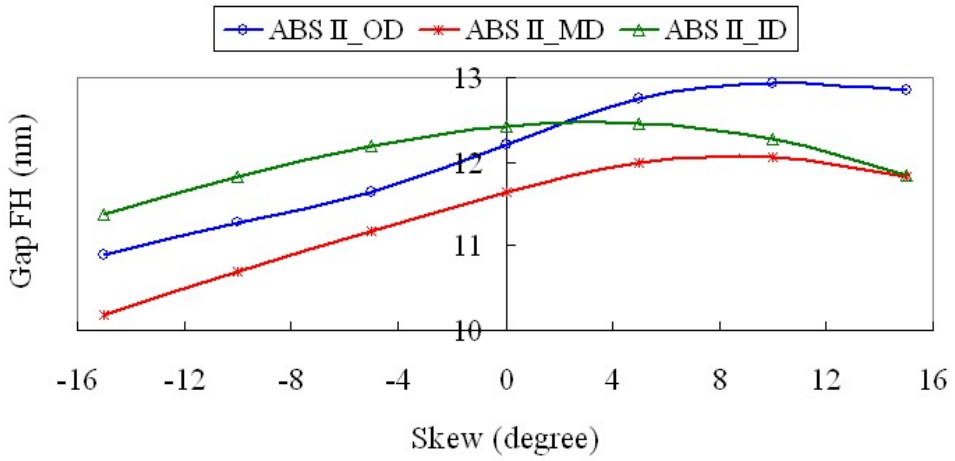

(a) ABS II

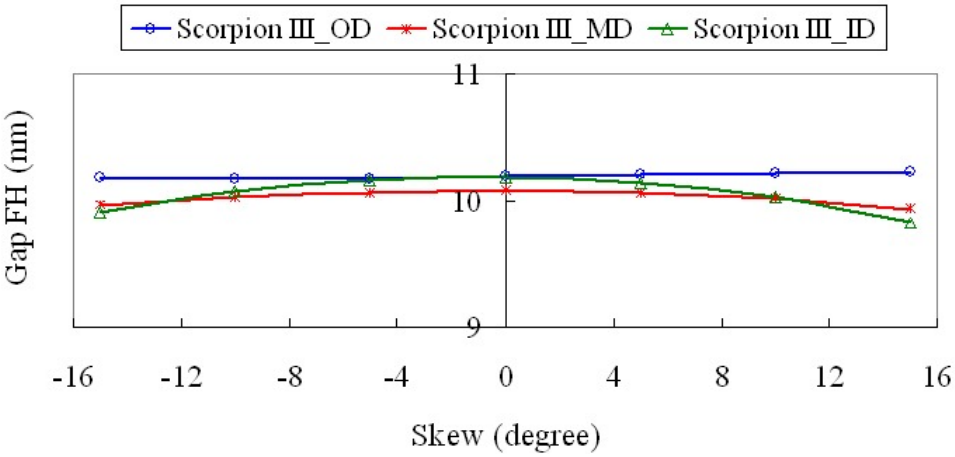

(b) Scorpion III

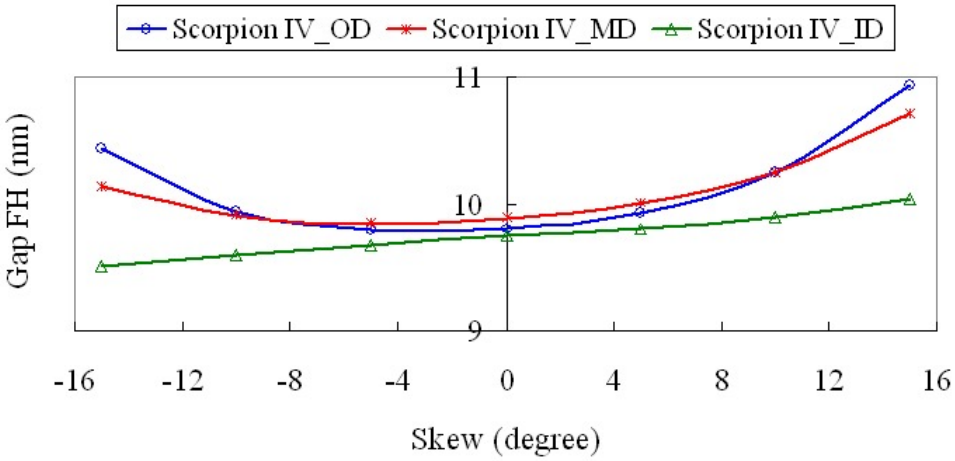

(c) Scorpion IV

Fig. 14. FH changes as a function of skew angle for (a) ABS II, (b) Scorpion III, and (c) Scorpion IV.

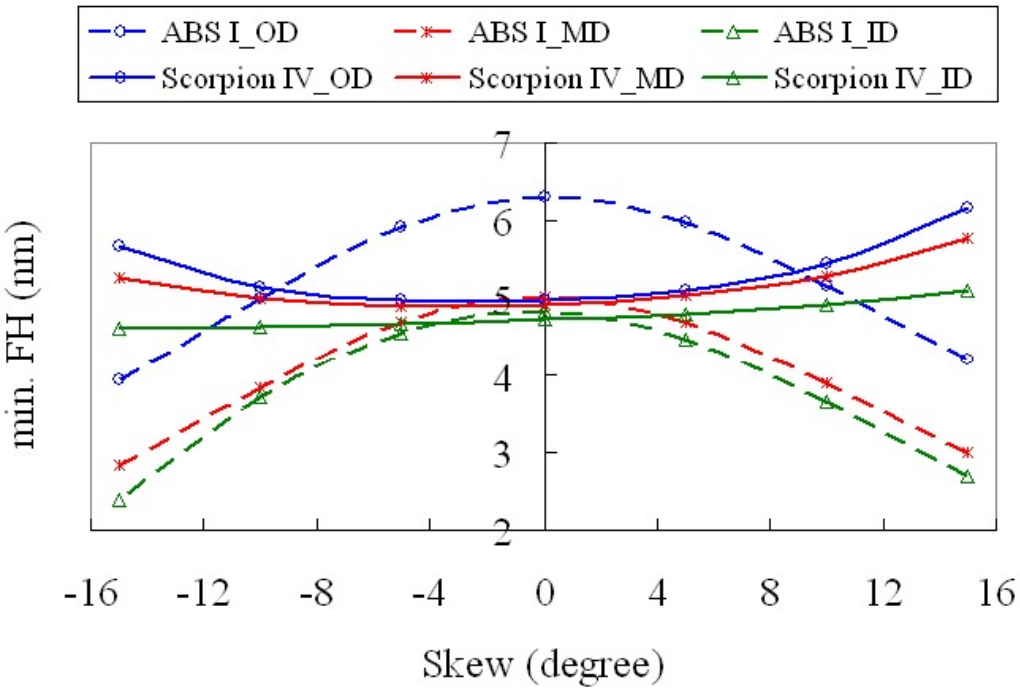

Fig. 15. A comparison of minimum FH changes as a function of skew angle between ABS I and Scorpion IV with a 4-nm actuation stroke.

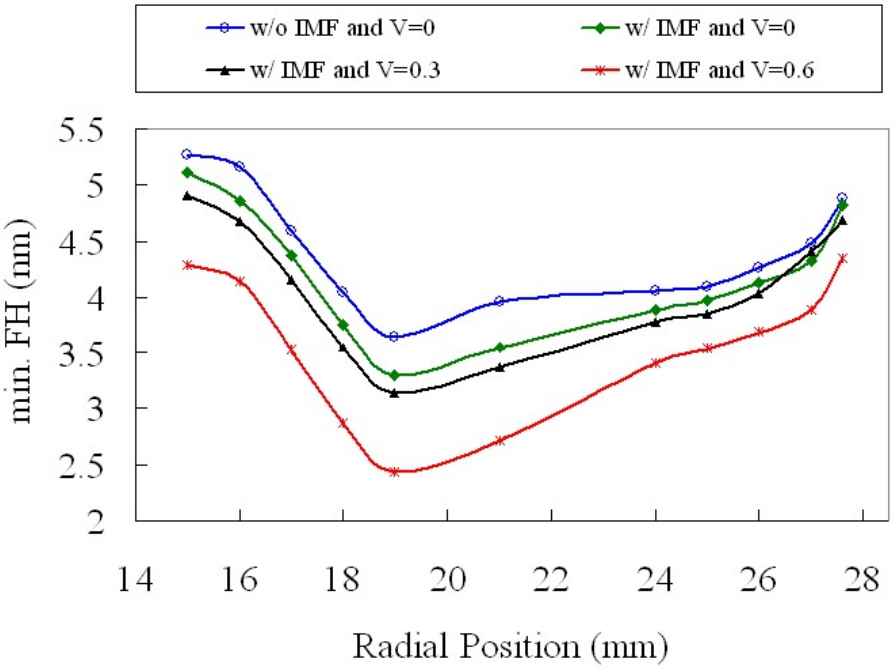

(a) ABS I

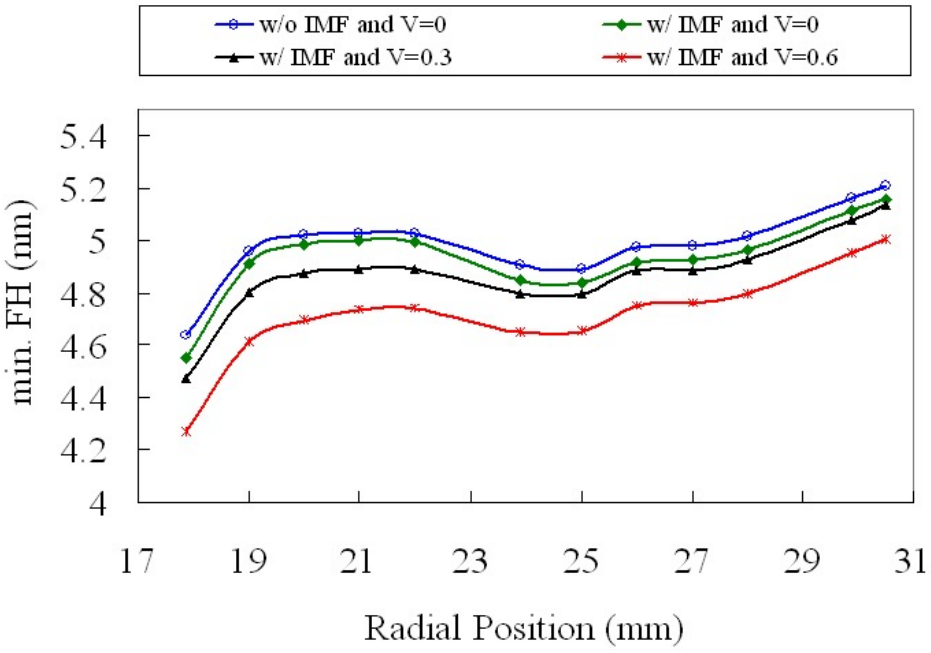

(b) Scorpion IV with a 4-nm actuation stroke

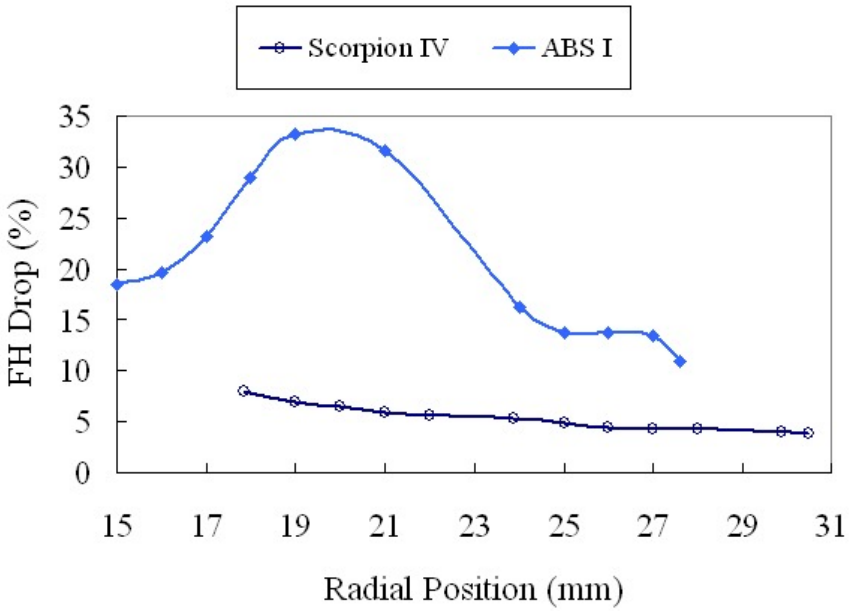

(c) with intermolecular forces and 0.6 V

Fig. 16. FH drops caused by the intermolecular and electrostatic forces during track-seeking motion (The Hamaker constant $A = 8.9 \times 10^{-20}$ J).